

# Simultaneous Imaging of Microglial Dynamics and Neuronal Activity in Awake Mice

Hisato Maruoka<sup>1</sup>, Ryosuke Kamei<sup>1</sup>, Shunsuke Mizutani<sup>1</sup>, Qingrui Liu<sup>1</sup>, Shigeo Okabe<sup>1</sup>

<sup>1</sup> Department of Cellular Neurobiology, Graduate School of Medicine and Faculty of Medicine, The University of Tokyo

## Corresponding Author

Shigeo Okabe

okabe@m.u-tokyo.ac.jp

## Citation

Maruoka, H., Kamei, R., Mizutani, S., Liu, Q., Okabe, S. Simultaneous Imaging of Microglial Dynamics and Neuronal Activity in Awake Mice. *J. Vis. Exp.* (186), e64111, doi:10.3791/64111 (2022).

## Date Published

August 23, 2022

## DOI

10.3791/64111

## URL

jove.com/video/64111

## Abstract

Since brain functions are under the continuous influence of the signals derived from peripheral tissues, it is critical to elucidate how glial cells in the brain sense various biological conditions in the periphery and transmit the signals to neurons. Microglia, immune cells in the brain, are involved in synaptic development and plasticity. Therefore, the contribution of microglia to neural circuit construction in response to the internal state of the body should be tested critically by intravital imaging of the relationship between microglial dynamics and neuronal activity.

Here, we describe a technique for the simultaneous imaging of microglial dynamics and neuronal activity in awake mice. Adeno-associated virus encoding R-CaMP, a gene-encoded calcium indicator of red fluorescence protein, was injected into layer 2/3 of the primary visual cortex in CX3CR1-EGFP transgenic mice expressing EGFP in microglia. After viral injection, a cranial window was installed onto the brain surface of the injected region. *In vivo* two-photon imaging in awake mice 4 weeks after the surgery demonstrated that neural activity and microglial dynamics could be recorded simultaneously at the sub-second temporal resolution. This technique can uncover the coordination between microglial dynamics and neuronal activity, with the former responding to peripheral immunological states and the latter encoding the internal brain states.

## Introduction

There is growing evidence that the internal state of the body constantly influences the brain functions in animals<sup>1,2,3,4,5</sup>.

Accordingly, to gain a deeper understanding of brain functions, it is crucial to elucidate how glial cells in the brain

monitor biological conditions in the periphery and relay the information to neurons.

Microglia, immune cells in the brain, are involved in synaptic development and plasticity, which sculpt characteristics of neural circuits in the brain<sup>6,7,8,9</sup>. For instance, the

pioneering work by Wake et al. demonstrated that microglial processes make contact with synapses in a neuronal activity-dependent manner in the mouse neocortex and that artificial ischemia induces synapse loss following prolonged contact with microglia<sup>10</sup>. Tremblay et al. found that alteration of visual experience changes the modality of microglial interaction with synapses. During the critical period when dendritic spine turnover in the primary visual cortex (V1) is increased by binocular deprivation, dark adaptation reduces the motility of microglial processes and increases both their contact frequency with synaptic clefts and the number of cellular inclusions in microglia<sup>11</sup>. These results suggest that microglial processes sense neural activity and their surrounding environment to remodel neural circuits. Furthermore, a recent study reported that microglial surveillance differs between awake and anesthetized conditions, suggesting the importance of experiments using awake mice for investigating neuron-microglia communication under physiological conditions<sup>12</sup>.

*In vivo* two-photon calcium imaging is a powerful tool for the recording of calcium dynamics, reflecting ongoing neuronal firing, in hundreds of neurons simultaneously in a living animal<sup>13,14,15</sup>. Calcium imaging in neurons generally requires a temporal resolution of more than a few Hz to track rapid neuronal responses<sup>16,17</sup>. In contrast, previous studies tracking microglial dynamics have sampled microglial structures at a relatively low temporal resolution of less than 0.1 Hz<sup>18,19,20</sup>. One recent study applied simultaneous two-photon imaging to understand neuron-microglia communication<sup>21</sup>. However, it is still unclear how dynamic microglial processes respond to the surrounding neural activity at a temporal resolution of more than a few Hz in awake mice. In order to address this issue, we describe a simultaneous *in vivo* two-photon imaging method of neural

activity and microglial dynamics with a temporal resolution higher than 1 Hz in awake mice. This method allows us to achieve stable imaging in awake mice at a higher frame rate (maximum, 30 Hz with the pixel frame size of 512 x 512 pixels) and provides a more favorable way to investigate the surveillance behavior of microglia or their interaction with neuronal activity in awake mice.

## Protocol

All experiments were approved by the Animal Ethics Committee and the Genetic Recombinant Experiment Safety Committee of Graduate School of Medicine and Faculty of Medicine, the University of Tokyo, and performed according to their guidelines.

### 1. Preparation

1. Sterilize all the instruments and apparatuses necessary for the surgery using autoclave or 70% ethanol.
2. Glass pipette preparation.
  1. Firmly fix a 75  $\mu$ L calibrated capillary to the holder of the micropipette puller. Set the puller to the program with the recommended parameters as P (pressure) = 500, HEAT = 680, PULL = 30, VEL = 60, TIME = 180.
  2. After finishing the program (usually 4.5 to 5 s), the capillary is divided into two glass pipettes with tapering tails. Then, break the distal part of the tails with tweezers to keep the tip diameter within 30-50  $\mu$ m. For this, break the tails 1 cm distal to the end of the beveled part.
3. For craniotomy, prepare a cranial window by gluing a larger outer glass disc, 4 mm in diameter, 0.15  $\pm$  0.02 mm in thickness, to a smaller inner glass disc, 2 mm in

diameter,  $0.525 \pm 0.075$  mm in thickness, using a UV light curing reagent (**Figure 2A**).

## 2. AAV injection

### 1. Preparation of injection apparatus

1. Place a glass pipette connected to a 26 G Hamilton syringe through a tube onto a pipette holder of a stereotaxic instrument, and then tilt the pipette holder  $60^\circ$  anteriorly from the vertical axis (**Figure 1A,B**).
2. Fill the glass pipette, the syringe, and the connecting tube with liquid paraffin. Place the syringe on a microinjector.

### 2. Surgical procedure

**NOTE:** The following surgery was performed in a sterilized booth. A stereomicroscope was used for the surgery if necessary.

1. Anesthetize a male CX3CR1-EGFP mouse (detailed information in the **Table of Materials**) at 7 to 8 weeks old (bodyweight 22-26 g) with 3% isoflurane in a gas-tight chamber. After 3 min, take out the mouse from the chamber when it loses voluntary movement except breathing, and then switch to continuous anesthesia by a nasal tube with 2% isoflurane.

**NOTE:** Isoflurane is known to activate microglia. However, because imaging is performed 4 weeks after the surgery, there is no effect of isoflurane on the mice during imaging. Although isoflurane anesthesia is used for a few minutes when mice are placed in the stereotaxic instrument before imaging (step 4.2.1), we found that the effect of this short anesthesia is negligible.

2. During surgery, keep the mouse warm with a heating pad at  $37^\circ\text{C}$  to prevent hypothermia. Apply eye ointment on both eyes to prevent corneal dryness and administer a meloxicam injection, subcutaneously (5 mg/kg). Attach the mouse to an auxiliary ear bar, and then fix the mouse on the stereotaxic instrument with its dorsal side up.
3. Adjust the isoflurane concentration to an appropriate percentage (1%-2%) during the surgery while monitoring the breath and heart rate. Remove the hair using depilatory cream and disinfect the head several times in a circular motion with both an iodine-based or chlorhexidine-based scrub and alcohol. Then, inject 0.1 mL of 1% lidocaine subcutaneously and apply sterile drapes to secure the surgical site.
4. Incise the scalp open along the midline with scissors and make the incision about 2 cm long, to ensure a good exposure of the skull above the right primary visual cortex. After the incision of the scalp, irrigate the head with saline throughout the whole procedure to prevent the exposed skull and brain from drying.
5. Remove the periosteum on the exposed skull using forceps. Drill the skull on the stereotaxic coordinates: 3 mm lateral to the midline, 0.5 mm anterior to the lambda line, to create a small hole with approximately 0.5 mm diameter. Rinse off blood and tissue debris from the drill bit, if necessary.
6. Fill the glass pipette with 1  $\mu\text{L}$  of rAAV2/1-hSyn-R-CaMP1.07 using the following procedure at a titer of  $8.3 \times 10^{12}$  vector genomes/mL<sup>22</sup>.
  1. Advance the syringe to eject 1  $\mu\text{L}$  of liquid paraffin from the glass pipette. Place a piece

of transparent film, approximately 2 cm x 2cm, on the exposed skull of the mouse and expel a droplet of 1  $\mu$ L of AAV solution on the film using a pipettor.

2. Place the glass pipette tip into the droplet of AAV solution on the film and gently pull the syringe to aspirate the AAV solution. After the ejection, turn the T-shape stopcock to release the pressure inside the tube and the glass pipette.
7. Insert the glass pipette to a depth of 500  $\mu$ m from the brain surface through the hole created in step 2.2.5, and then inject 0.5  $\mu$ L of AAV solution using the microinjector (**Figure 1C**). Use the injection volume flow rate of 2.0  $\mu$ L/h; an injection of 0.5  $\mu$ L takes 15 min, and then subsequently wait for 5 min.
8. After the injection, gently withdraw the glass pipette and rinse the brain surface with saline.

### 3. Cranial window implantation

**NOTE:** Cranial window implantation follows the AAV injection on the same day.

1. Mark a 2.5 mm diameter circle on the skull, centered 3 mm laterally from the lambda. Create a circular groove along the mark on the skull by drilling. Clean the debris as it may adversely affect the visibility of the skull and apply saline during the drilling process to prevent heating up.
2. To check whether the drilling depth in the circular groove is sufficient to remove the central skull fragment, gently press the central skull with forceps. If it moves vertically with little resistance, the drilling depth is sufficient.
3. When the groove reaches enough depth, insert the tip of the forceps into the bottom of the central skull fragment

and gently lift and remove it to expose the brain surface (**Figure 1D**).

4. Using a 27 G needle, prick and tear the dura at the edge of the exposed brain surface. Insert the tip of the forceps through the hole made at the edge of the dura. Hold the dura and peel it off to expose the brain surface.
 

**NOTE:** If bleeding occurs, rinse the brain surface with saline until the bleeding stops.
5. Using forceps, disperse hemostatic fibers one by one in saline in a 3.5 mm dish, and then place the hemostatic fibers along the margins of the hole in which the transected dura is present.
6. Place a cranial window prepared in step 1.3 on the exposed brain surface, and then adhere it to the skull with instant glue while gently pressing the window so that the window is in close contact with the skull.
7. Afterward, apply instant glue to the whole exposed skull, and then carefully attach a head-plate onto the skull so that the window locates at the center of the square hole of the head-plate (**Figure 2C**). Ensure that the surface of the head plate is parallel to the surface of the glass window.
8. After the glue has sufficiently hardened, apply dental cement to the exposed skull to reinforce the attachment between the head and the head-plate (**Figure 2**).
 

**NOTE:** If the experiments include the presentation of visual stimuli to mice, stray light to the imaging area should be avoided. It is advisable to blacken the cement by mixing it with the activated charcoal for the reduction of light reflection.
9. Withdraw the mouse from the anesthesia after the cement has hardened sufficiently (about 20 min). Then, put the mouse into a new cage to recover alone.

10. After confirming its consciousness and voluntary movement, indicating full recovery, put the mouse back in the home cage. During the recovery, administer a second, or more if necessary, meloxicam dose (once every 24 hours for 1-3 days) if obvious pain-indicating behaviors occur.

#### 4. *In vivo* two-photon imaging of microglia and neuronal calcium dynamics

1. Habituation of mice to the microscope apparatus
  1. Three weeks after the surgery, induce anesthesia in the mouse with 3% isoflurane, and set the mouse under the 25x objective lens of a two-photon microscope using a custom-made stereotaxic instrument (**Figure 3C**). For the setup here, the mouse is set on the top of a treadmill and allowed to run freely.
  2. Approximately 10 min later, remove the mouse from the microscope stage and return it to the home cage. Repeat the habituation at least 3 times every alternate day before two-photon image acquisition.
2. Two-photon image acquisition
 

**NOTE:** We recommend performing the image acquisition more than 4 weeks after surgery, as microglial activation gradually returns to the basal level.

  1. As in step 4.1, induce anesthesia in the mouse with 3% isoflurane and set the mouse under the objective lens of the two-photon microscope using a custom-made stereotaxic instrument.
  2. Install the custom-made shading device and an LCD monitor for visual stimulation as described below (**Figure 3D**).

1. Position the lens to focus on the brain surface, and then set this lens position as the original Z-position. Keep the x-y coordinates constant and elevate the objective lens; remove the mouse and stereotaxic instrument from the objective lens and treadmill.
2. Attach a shading device on the top of the head plate using silicone, which is blackened by mixing with charcoal powder, and ensure the space between the head plate and the shading device is well-sealed.
3. Fill the shading device with distilled water, and then fix the mouse and the stereotaxic frame again under the objective and on the treadmill. Carefully reset the focal plane at the brain surface, checking the depth of the objective lens.
 

**NOTE:** To avoid the risk of damaging the objective lens, set the xyz coordinates first, and then apply the shading device of the objective lens. It is also reasonable to install the cover first, and then adjust the coordinates, but cautious handling is necessary for this option.
4. Cover the objective lens with black aluminum foil to avoid light contamination from the LCD monitor used for visual stimulation through the objective lens (**Figure 3D**). Set a 10-inch LCD monitor at 12.5 cm in front of the mouse's eyes to present visual stimuli (**Figure 3D**).
3. Configure the fluorescence emission collection filters to EGFP fluorescence (525/50 nm emission filter) and R-CaMP fluorescence (593/46 nm emission filter) and the excitation wavelength to

1,000 nm. Acquire images with the spatial resolution of 0.25  $\mu\text{m}/\text{pixel}$  using a 25x 1.1 NA objective and GaAsP PMTs.

4. Find the imaging region in which R-CaMP(+) neurons and EGFP(+) microglia can be simultaneously imaged in layer 2/3. For this setup, data obtained in **Figure 4** and **Video 1** were at a depth of 100  $\mu\text{m}$  from the pial surface, using a live image preview. Keep the power of the excitation laser as low as possible to avoid photo-bleaching and damage caused by increased local temperature in the imaging region.
5. Acquire images at the frame rate of 30 Hz. Simultaneously with the image acquisition, present a drifting-grating visual stimuli at 100% contrast, 1.5 Hz, 0.04 cycles per degree in 12 directions at 6 orientations from 0° to 150° in 30° steps to the mouse<sup>17</sup>.
6. After the image acquisition, remove the mouse from the microscope stage, detach the shading device and the stereotaxic instrument from the mouse, and return the mouse to its home cage.

### 3. Data registration

1. Convert and save the acquired image data (nd2 format in this case) as a series of tiff image files for each color channel, using Fiji or the software supplied with the microscope.
2. Apply Turboreg, a plugin of Fiji, to perform registration with mode = translation. Use averaged image as the reference image with the tiff image files of EGFP channel.
3. Perform the following processing for each frame using MATLAB.

**NOTE:** Although MATLAB is used in the following processing, the description mainly focuses on the intention of each step so that data can be analyzed by other programming software such as Python.

1. Use the imread function to read two EGFP tiff images before and after registration of the same frame, respectively. Use the imread function to read the R-CaMP tiff image of the same frame.
  2. Use the normcorr2 function to calculate the correlation function between the vectorized variables of the two GFP images read in step 4.3.3.1.
  3. Use the max function to detect the linear index with the highest cross-correlation of the correlation function, and then use the ind2sub function to calculate the movement position of the registered image from its original image.
  4. Use the imwarp function to translate the R-CaMP image to the position calculated in step 4.3.3.3, and then use the imwrite function to save the registered image of R-CaMP.
- ### 4. Generation of calcium traces
1. Perform the following processing using MATLAB. Use the imread function to read all the registered R-CaMP tiff images generated in step 4.3.3.4. If the registered images have been already loaded as a variable in workspace, omit this step.
  2. Use the mean function to generate a time-projection image. Use the imshow function to show the averaged image as a figure; use the roipoly function to generate a binary ROI mask of the target structure (dendritic spine in this data).

3. Using the mean function with the images obtained by multiplying the binary mask with images of each frame as input variables, calculate the averaged fluorescence intensity within the ROI for each frame.
4. As described previously<sup>17</sup>, to the variable obtained in step 4.4.3, apply the butter worth frequency filter at cutoff = 1.6 s, for cutting high-frequency noise, and then apply the sliding median filter at the time window = 200 s, for cutting low-frequency noise.

### Representative Results

We performed the AAV injection and cranial window implantation in V1 of an 8-week-old CX3XR1-EGFP transgenic mouse as described in this protocol. Four weeks after the surgery, we performed simultaneous *in vivo* two-photon imaging of R-CaMP-based neural activity and microglial dynamics in layer 2/3 of V1 (**Figure 4** and **Video**

**1**). During the imaging, the mouse was placed on a treadmill and allowed to run freely. Images were acquired at the frame rate of 30 Hz with the spatial resolution of 0.25  $\mu\text{m}$ /pixel using a 25x, 1.1 NA objective and GaAsP PMTs. Both EGFP and R-CaMP were excited at a wavelength of 1,000 nm, and EGFP fluorescence (525/50 nm emission filter) and R-CaMP fluorescence (593/46 nm emission filter) were collected simultaneously. After the registration of acquired data to minimize motion artifacts, every four frames were averaged into one frame to reduce background noise. Grating visual stimuli were presented to the mouse, and the visual responses of neurons and individual dendritic spines were analyzed (**Figure 4D**). Microglial processes showed fast dynamics and changed their morphology within 10 s (**Figure 4E** and **Video 1**). As detailed in the Discussion section, when the AAV injection failed, the expression of R-CaMP could not be detected. If the surgery was not successful, the signals of EGFP and R-CaMP could not be observed.

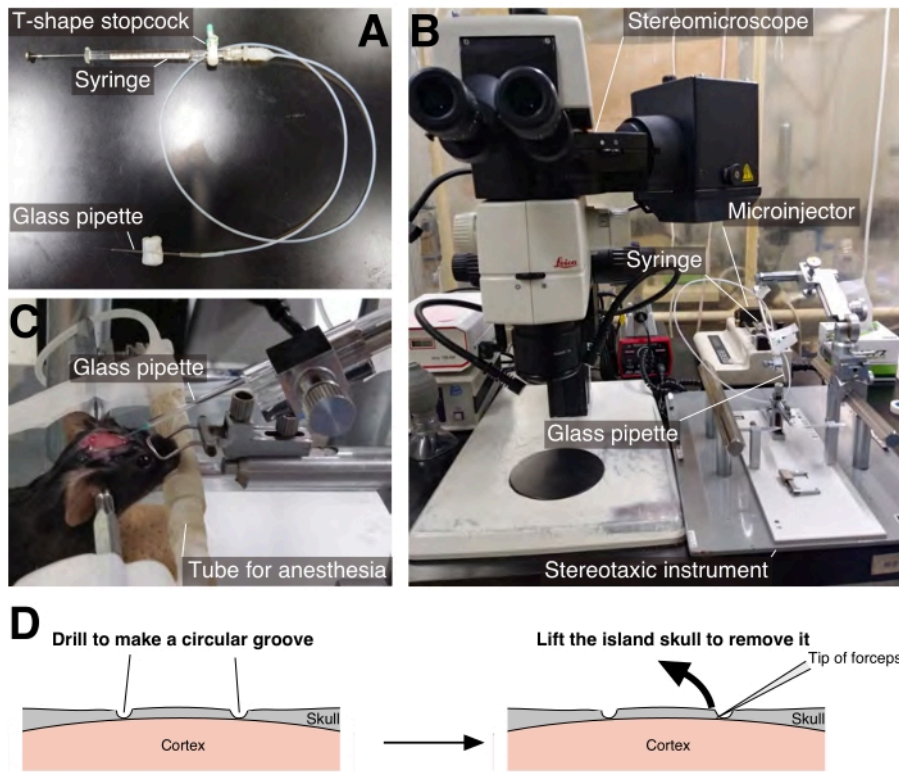


**Figure 1: AAV injection.** (A) A glass pipette was connected to a 26 G Hamilton syringe using a silicon tube. (B) The set-up for AAV injection. (C) AAV solution was injected *via* the glass pipette tilted 60° anteriorly from the vertical axis. (D) Schematic diagram of the procedure of open skull (described in step 3.3). [Please click here to view a larger version of this figure.](#)

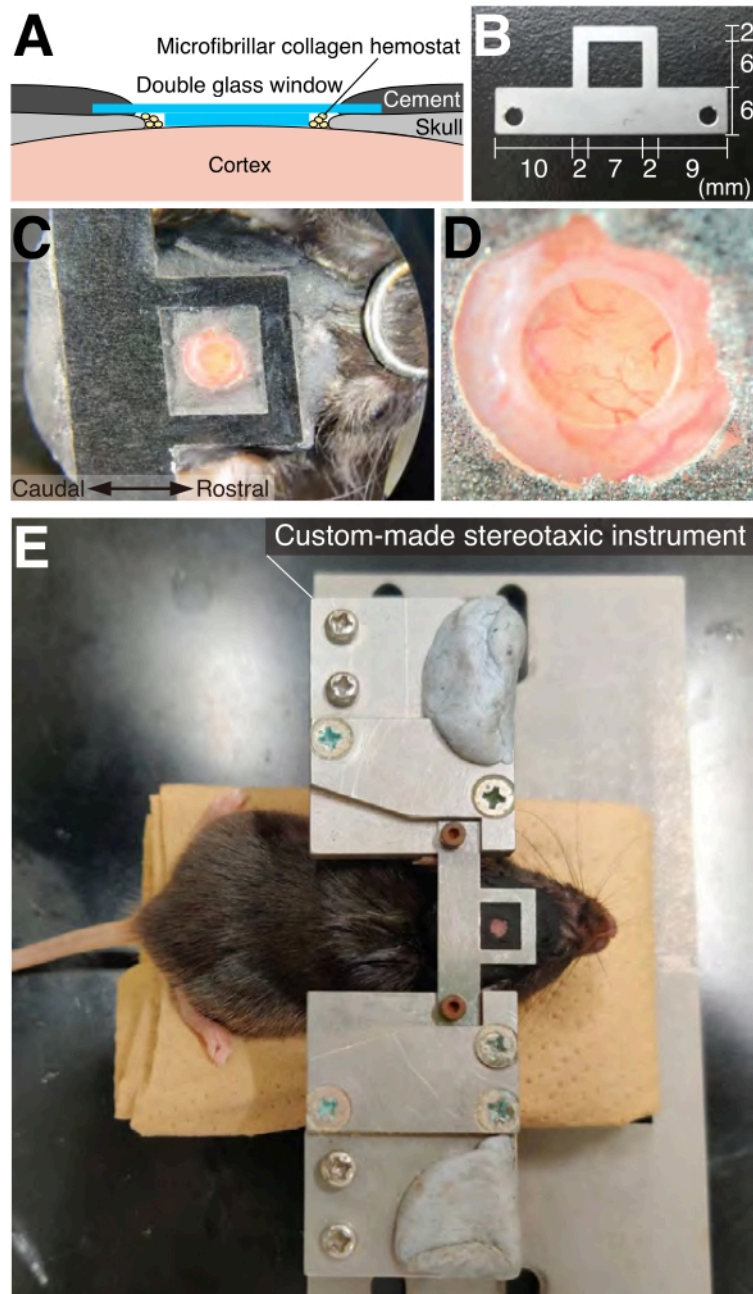


**Figure 2: Cranial window and head-plate.** (A) Schematic diagram of cranial window implantation. (B) Custom-made head-plates were used. For imaging in the right hemisphere, the shorter arm should be used on the right side. (C) Dorsal view of a mouse with a cranial window and an implanted head plate. (D) High magnification view of the cranial window shown in Figure 2C. (E) Dorsal view of a mouse fixed with the custom-made stereotaxic instrument. [Please click here to view a larger version of this figure.](#)

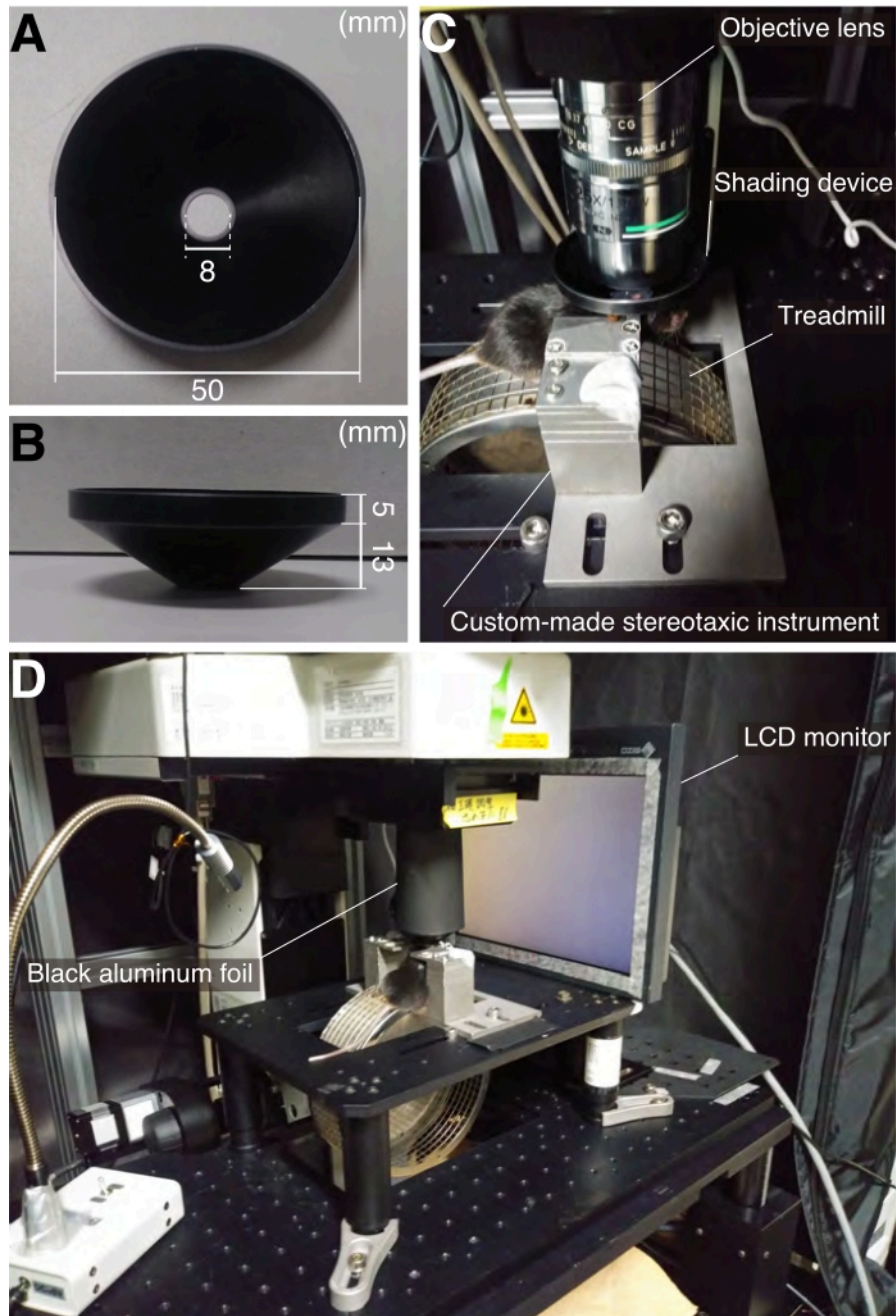


**Figure 3: The set-up for *in vivo* two-photon imaging.** (A) Dorsal view of shading device. (B) Side view of shading device. (C) View of a mouse with the shading device on the head plate under the objective lens. The mouse is placed on the treadmill. (D) View under the two-photon excitation microscope. A monitor presenting visual stimuli is placed on the right side of the figure. The objective lens is covered with the shading device and black aluminum foil to avoid light from the monitor to the objective lens. [Please click here to view a larger version of this figure.](#)

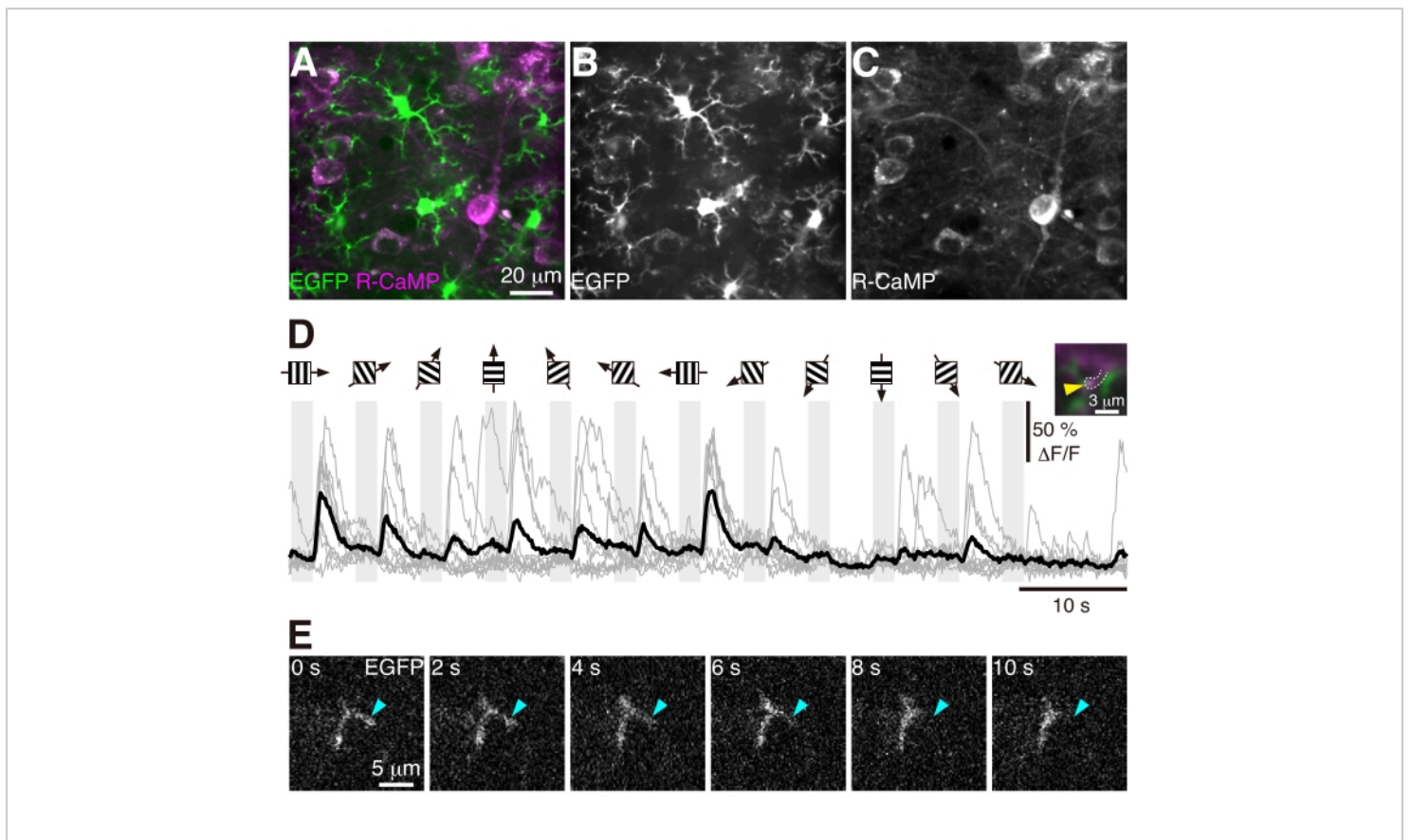


**Figure 4: Microglial dynamics and visual responses in a dendritic spine.** (A-C) Time-averaged images of EGFP(+) microglia and R-CaMP(+) neurons in layer 2/3 of V1 in a 12-week-old CX3XR1-EGFP transgenic mouse. Signal intensity in each channel was normalized independently. (D) Visual responses in a dendritic spine. Stripe diagrams with black arrows indicate the direction of the grating stimuli presented in the timing indicated by gray columns. In calcium traces, gray lines indicate individual responses, and a black line indicates their average. In the right inset, a yellow arrowhead indicates the dendritic spine in which the region of interest (ROI) was generated to acquire the calcium traces. (E) Microglial process (cyan arrowhead) showed rapid retraction in 10 s. [Please click here to view a larger version of this figure.](#)

**Video 1: Two-photon imaging of neuronal activity and microglial dynamics.** Imaging data of EGFP(+) microglia and R-CaMP(+) neurons in layer 2/3 of V1 in a 12-week-old CX3XR1-EGFP transgenic mouse. On the left side of the movie, magenta indicates R-CaMP in neurons, and green indicates EGFP in microglia. The center of the movie corresponds to the EGFP signal, and the right side corresponds to the R-CaMP signal. Signal intensity in each

channel was normalized independently. The frame rate of the movie is 40 times faster than the actual rate. Scale bar = 10  $\mu\text{m}$  [Please click here to download this Video.](#)

## Discussion

We describe the protocol of AAV injection and craniotomy for simultaneous imaging of microglial dynamics and neuronal activity in awake mice as well as data processing. This

technique can uncover the coordination between microglial dynamics and neuronal activity on time scales ranging from sub-second to tens of seconds.

The surgery protocol involves several technically demanding steps. AAV injection is one of the critical steps. Unsuccessful AAV injection may cause a significant reduction in the expression of R-CaMP. There are two main reasons: clogged glass pipettes and tissue damage. The clogging of glass pipettes reduces or completely blocks the ejection of AAV solution. This situation can be avoided by coloring the AAV solution with a dye such as fast green and visually confirming the success of the injection. Tissue damage caused by AAV injection prevents exogenous gene expression near the center of the injection site. The damage induced by AAV injection is likely to be caused by a sudden increase in the efflux from the tip of the glass pipette after the accumulation of the pressure inside the pipette. Therefore, the outflow of AAV solution from the glass pipette should be constant during the injection. Selecting glass pipettes with a slightly wider diameter at their tips would solve this problem. In cranial window implantation, the speed of surgery is critical. If the surgery takes too long, the brain tissue can be severely damaged. Accordingly, repeated practice is necessary to ensure the speed and smoothness of surgery. In addition, during the 4 weeks from surgery to imaging, the quality of imaging may be reduced by tissue regeneration between the cranial window and the brain tissue by the conventional method<sup>17</sup>. The method here overcomes this issue by applying thick glasses for the inner glass disc of the cranial windows to inhibit tissue regeneration and keep the window clear. In the system described here, this effect was evident by using an inner glass disc with a thickness of  $0.525 \pm 0.075 \mu\text{m}$ .

The method can be applied successfully to mice older than 4 weeks, but the application to younger mice may be problematic. In juvenile mice, the skull shows rapid and prominent growth, which induces a mismatch between the cranial bone and the glass window.

In some cutting-edge studies, *in vivo* two-photon imaging was used to study microglia-neuron interactions<sup>12,21,23</sup>. Especially in the pioneering work by Merlini et al., they performed simultaneous *in vivo* imaging of microglial dynamics and neural activity within the cell bodies<sup>21</sup>. In this method, by using thicker inner glasses for cranial windows, we could suppress motion artifacts in the depth orientation and achieve the stable measurement of neuronal activity in microstructures, such as dendritic spines. This method would help investigate synapse-microglial process interactions in awake mice.

Recently, *in vitro* study demonstrated that thin filopodia-like microglial processes have faster motility than thick processes, suggesting the importance of their faster motility in surveillance<sup>19</sup>. The system here can track the motility of thin microglial processes with a temporal resolution from a sub-second to a few tens of seconds. This property helps elucidate the functional significance of their motility for surveillance *in vivo*.

In the future, the combination of this imaging technique with interventions, such as optogenetics<sup>24</sup> or chemogenetics<sup>25</sup>, applied to local neural circuits or interregional neural connections would shed light on novel microglial functions in synaptic development and plasticity which sculpt characteristics of neural circuits. Also, further integration of imaging, intervention, and behavioral tasks would contribute

to revealing the coordination of microglia and neurons underlying specific behaviors.

## Disclosures

The authors have nothing to disclose.

## Acknowledgments

We thank Dr. Masashi Kondo and Dr. Masanori Matsuzaki for providing virus vectors. This work was supported by Grants-in-Aid for Scientific Research (20H00481, 20A301, 20H05894, 20H05895 to S.O.), the Japan Agency for Medical Research and Development (JP19gm1310003 and JP17gm5010003 to S.O. and JP19dm0207082 to H.M.), the UTokyo Center for Integrative Science of Human Behavior (CiSHuB), the Japan Science and Technology Agency Moonshot R&D (JPMJMS2024 to H.M.), Brain Science Foundation (to H. M.).

## References

1. Andoh, M. et al. Exercise reverses behavioral and synaptic abnormalities after maternal inflammation. *Cell Reports*. **27** (10), 2817-2825.e5 (2019).
2. Inoue, K., Tsuda, M. Microglia in neuropathic pain: cellular and molecular mechanisms and therapeutic potential. *Nature Reviews. Neuroscience*. **19** (3), 138-152 (2018).
3. Clasadonte, J., Scemes, E., Wang, Z., Boison, D., Haydon, P. G. Connexin 43-mediates astroglial metabolic networks contribute to the regulation of the sleep-wake cycle. *Neuron*. **95** (6), 1365-1380 (2017).
4. Taylor, A. M. W. et al. Microglia disrupt mesolimbic reward circuitry in chronic pain. *Journal of Neuroscience*. **35** (22), 8442-8450 (2015).
5. Kondo, S., Kohsaka, S., Okabe, S. Long-term changes of spine dynamics and microglia after transient peripheral immune response triggered by LPS in vivo. *Molecular Brain*. **4**, 27 (2011).
6. Wu, Y., Dissing-Olsen, L., MacVicar, B. A., Stevens, B. Microglia: Dynamic mediators of synapse development and plasticity. *Trends in Immunology*. **36** (10), 605-613 (2015).
7. Andoh, M., Koyama, R. Microglia regulate synaptic development and plasticity. *Developmental Neurobiology*. **81** (5), 568-590 (2020).
8. Iida, T., Tanaka, S., Okabe, S. Spatial impact of microglial distribution on dynamics of dendritic spines. *European Journal of Neuroscience*. **49** (11), 1400-1417 (2019).
9. Nakayama, H. et al. Microglia permit climbing fiber elimination by promoting GABAergic inhibition in the developing cerebellum. *Nature Communications*. **9** (1), 2830 (2018).
10. Wake, H., Moorhouse, A. J., Jinno, S., Kohsaka, S., Nabekura, J. Resting microglia directly monitor the functional state of synapses in vivo and determine the fate of ischemic terminals. *Journal of Neuroscience*. **29** (13), 3974-3980 (2009).
11. Tremblay, M. E., Lowery, R. L., Majewska, A. K. Microglial interactions with synapses are modulated by visual experience. *PLoS Biology*. **8** (11), e10000527 (2010).
12. Liu, Y. U. et al. Neuronal network activity controls microglial process surveillance in awake mice via norepinephrine signaling. *Nature Neuroscience*. **22** (11), 1771-1781 (2019).

13. Kim, T. H., Schnitzer, M. J. Fluorescence imaging of large-scale neural ensemble dynamics. *Cell*. **185** (1), 9-41 (2022).
14. Grienberger, C., Konnerth, A. Imaging calcium in neurons. *Neuron*. **73** (5), 862-885 (2012).
15. Isshiki, M., Okabe, S. Evaluation of cranial window types for in vivo two-photon imaging of brain microstructures. *Microscopy (Oxf)*. **63** (1), 53-63 (2014).
16. Ohtsuki, G. et al. Similarity of visual selectivity among clonally related neurons in visual cortex. *Neuron*. **75** (1), 65-72 (2012).
17. Maruoka, H. et al. Lattice system of functionally distinct cell types in the neocortex. *Science*. **358** (6363), 610-615 (2017).
18. Nimmerjahn, A., Kirchhoff, F., Helmchen, F. Resting microglial cells are highly dynamic surveillants of brain parenchyma in vivo. *Science*. **308** (5726), 1314-1318 (2005).
19. Bernier, L. P. et al. Nanoscale surveillance of the brain by microglia via cAMP-regulated filopodia. *Cell Reports*. **27** (10), 2895-2980.e4 (2019).
20. Sun, W. et al. In vivo two-photon imaging of anesthesia-specific alterations in microglial surveillance and photodamage-directed motility in mouse cortex. *Frontiers in Neuroscience*. **13**, 421 (2019).
21. Merlini, M. et al. Microglial G<sub>i</sub>-dependent dynamics regulate brain network hyperexcitability. *Nature Neuroscience*. **24** (1), 19-23 (2021).
22. Kondo, M., Kobayashi, K., Ohkura, M., Nakai, J., Matsuzaki, M. Two-photon calcium imaging of the medial prefrontal cortex and hippocampus without cortical invasion. *eLife*. **6**, e26839 (2017).
23. Badimon, A. et al. Negative feedback control of neuronal activity by microglia. *Nature*. **586** (7829), 417-423 (2020).
24. Rajasethupathy, P., Ferenczi, E, Deisseroth, K. Targeting neural circuits. *Cell*. **165** (3), 524-534 (2016).
25. Roth, B. L. DREADDs for Neuroscientists. *Neuron*. **89** (4), 683-694 (2016).